 ©2016 Kvantovaya Elektronika and Turpion Ltd

DOI: 10.1070/QEL15811

Microstructure of the multiple-filamentation zone formed by femtosecond laser radiation in a solid dielectric

Yu.E. Geints, S.S. Golik, A.A. Zemlyanov, A.M. Kabanov, A.V. Petrov

Abstract. **The regularities of multiple filamentation of gigawatt femtosecond laser pulses in a solid dielectric (optical glass) have been considered. The fine spatial structure of the plasma region that is formed under glass photoionisation and accompanies the formation of light filaments is analysed experimentally and by means of numerical simulation. The dependence of the number, position, and extension of individual 'generations' of plasma channels on the laser pulse energy has been investigated for the first time. It is found that the distribution of the number of plasma channels over the length of a dielectric sample has a maximum, the position of which correlates well with the position of the nonlinear focus of the light beam as a whole; at the same time, the average channel length decreases with increasing pulse power, whereas the number of successive channel 'generations', on the contrary, increases.**

Keywords: *multiple filamentation of femtosecond laser radiation, solid dielectric, plasma channels.*

1. Introduction

Filamentation is a striking manifestation of self-focusing [1] of high-power laser radiation propagating in a medium with cubic optical (Kerr) nonlinearity. The radiation self-action leads to spatial decomposition of the light-beam transverse profile into localised high-intensity zones (filaments). Visual signs of beam filamentation are the occurrence of extended luminous plasma channels along the propagation path and generation of extremely broadband radiation: supercontinuum. Plasma is formed as a result of ionisation of a medium by radiation, which is highly intense in filamentation zones. The state of the art of the studies in this field is described, for example, in reviews [2–4].

To pass to the filamentation regime, a laser beam must overcome natural diffraction, which leads to its expansion during propagation in a medium. This circumstance imposes a certain threshold condition on the beam power at a specified wavelength. For example, in air under normal pressure, the threshold (or critical) self-focusing power P_c in the micrometre wavelength range is on the order of several GW. In transparent liquids (water, ethanol) and solid dielectrics (quartz, optical glass), this value is generally several thousands of times smaller.

The initial peak power P_0 of radiation determines in the long run the number of filaments produced in a medium and the plasma-channel structure corresponding to these filaments. If the initial beam peak power greatly exceeds the critical level ($P_0 \gg P_c$), many filaments are simultaneously formed [5–7]. Multiple filamentation (MF) is a random process in many respects, because its development is significantly affected by the small-scale self-focusing of the spatial and temporal profile of the laser beam on random inhomogeneities [5, 8] and by the optical inhomogeneity of the propagation medium [9, 10].

Many studies of different research teams were devoted to the theoretical analysis of the laser beam MF in media with different physical characteristics (the corresponding references can be found, e.g., in reviews [2–4]). The key point of the MF theoretical model is the concept of 'optical turbulence' [6], which is implemented under conditions of multiple self-focusing of light. This means that the MF of a high-power laser pulse, similar to the evolutionary processes occurring in other physical systems under strong turbulence conditions, has generally a stochastic character. The physical pattern of MF evolution in a regular air medium – the diffractive interaction of individual filaments, which leads either to the occurrence of new ('daughter') filaments or to the suppression of existing ones – was investigated in [11, 12]. The statistical characteristics of the evolution of filaments upon laser beam MF in a turbulent atmosphere were reported in [13].

This, rather complicated and unstable (from pulse to pulse) turbulent pattern of laser beam MF, where filaments and plasma channels formed by them exhibit significant variability of their spatial position and transverse size along the propagation path, is characteristic specifically of gas media and near-IR laser radiation [11] (filamentation of UV light in air is characterised by reproducible transverse distribution of filaments [14]).

At the same time, the MF pattern in condensed (liquids) and solid media is apparently characterised by higher stability. When the self-focusing critical power is significantly exceeded, groups of filaments arise as a result of small-scale self-focusing of the light beam, which form parallel plasma channels in the medium [15–18]; these channels retain their transverse position in the beam. In addition, experiments showed that an individual plasma channel (and the light filament generating it) may be interrupted and arise again several times in the same area of the light beam cross section [17], thus demonstrating the so-called light focusing–refocusing

Yu.E. Geints, A.A. Zemlyanov, A.M. Kabanov, A.V. Petrov V.E. Zuev Institute of Atmospheric Optics, Siberian Branch, Russian Academy of Sciences, pl. Akad. Zueva 1, 634021 Tomsk, Russia;
e-mail: ygeints@iao.ru;
S.S. Golik Institute of Automatics and Control Processes, Far Eastern Branch, Russian Academy of Sciences, ul. Radio 5, 690041 Vladivostok, Russia

Received 20 March 2015; revision received 30 November 2015
Kvantovaya Elektronika **46** (2) 133–141 (2016)
Translated by Yu.P. Sin'kov

cycles [18]. The number of refocusings, producing successive 'generations' of plasma channels, depends directly on the peak pulse power. However, this problem has not been addressed in detail, and some other statistical characteristics of the plasma channels accompanying a laser pulse undergoing filamentation in a solid dielectric, have not been determined either.

In this paper, we report the results of studying the fine spatial structure of the plasma region formed by a high-power laser beam in a medium during its propagation in the MF regime. Experimental measurements were performed with optical glass BK7. The model medium in the theoretical calculations was chosen to be fused silica, which has a cubic nonlinearity coefficient of the refractive index close to that of glass. To the best of our knowledge, the spatial configuration, number, position and length of different generations of plasma channels, as well as their dependence on the laser beam energy, were investigated for the first time. The main purpose of our study was to gain a deeper insight into the physical nature of small-scale random MF of high-power radiation in a nonlinear medium (specifically, to analyse the spatial variability of the plasma region in the laser-beam channel). As a result, we revealed a close-to-unimodal distribution of plasma linear density along the dielectric sample length, with a maximum correlating with the position of the laser-beam nonlinear focus. It was found that the number of generations of plasma channels increases with an increase in the radiation energy, and the extension of plasma channels in each generation is characterised by a large spread: from several micrometres to several tens of millimetres. At the same time, the average length of channels decreases with an increase in the pulse power.

2. Experimental results

Experiments were performed on a bench of the Institute of Automatics and Control Processes, Far Eastern Branch, Russian Academy of Sciences. We used the fundamental harmonic (centre wavelength $\lambda_0 = 800$ nm) of a Ti : sapphire laser (Spitfire Pro40F, Spectra Physics) with the following parameters: full width at half maximum (FWHM) of individual pulses 45 fs, their repetition frequency 1 kHz, beam diameter 9 mm (at a level of e^{-2}), maximum pulse power P_0 up to 120 GW, and energy E_0 up to 5.4 mJ.

A laser pulse was directed to a rectangular (80 × 40 × 40 mm) BK7 glass sample (with a near-IR refractive index of 1.51). When the power reached a certain level, the pulse underwent self-focusing and filamentation in the glass sample. The lateral luminescence (of pronounced blue-green colour) from the filamentation zone was recorded by an ANDOR-Clara E CCD camera, equipped with an HELIOS-44M 2/58 objective and located on a linearly moving platform, which made it possible to observe successively the entire filamentation zone. Since the sample was not entirely fit into the objective field of view, the camera was moved in the longitudinal direction, and parts of the glass bar with a field-of-view length of 25 mm were successively imaged. The thus obtained individual frames were matched in a graphical editor, and the resulting image was then processed within the special program package Profilometer [19].

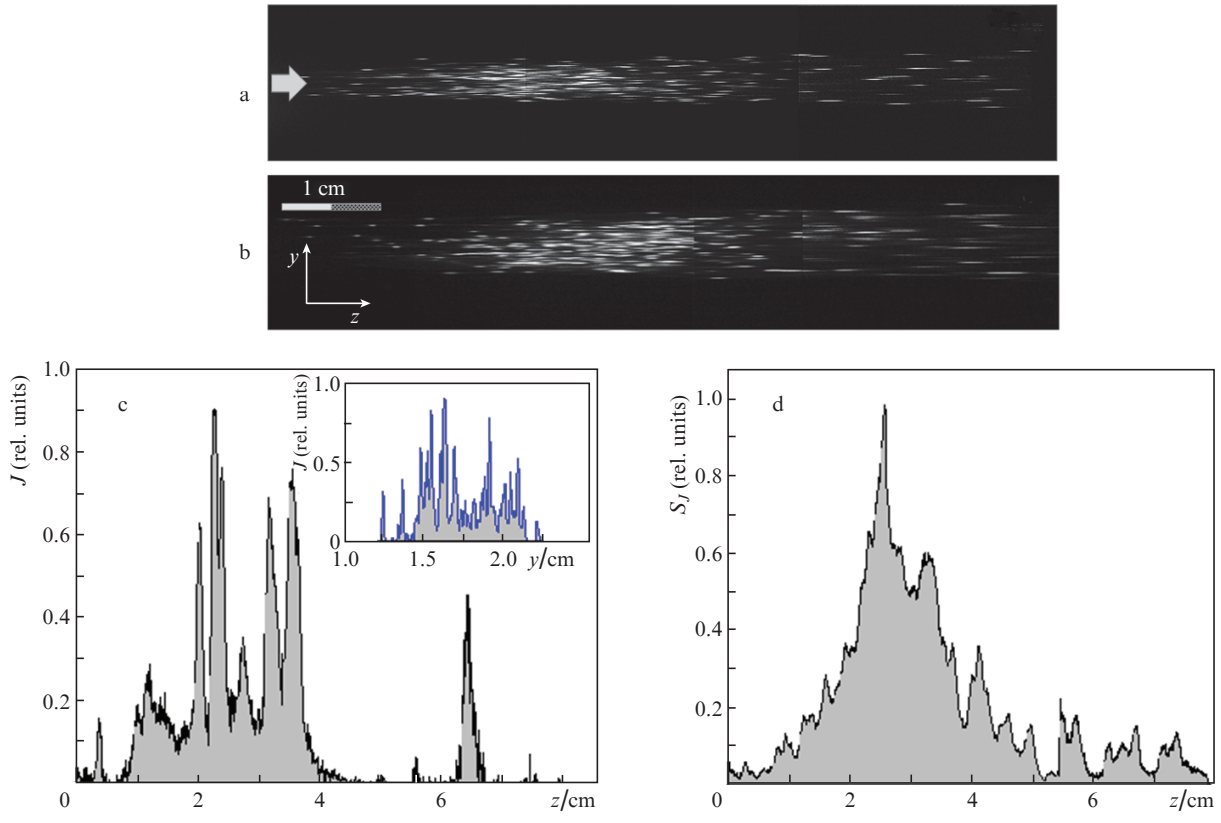

Figure 1. (a, b) Images of a laser beam filamentation zone in a glass bar at E_0 = (a) 3 and (b) 4.5 mJ, (c) the luminescence intensity profile J for plasma channels at $E_0 = 3$ mJ along the bar axis (the inset shows a transverse intensity profile at $z = 3$ cm), and (d) the integral luminescence intensity S_J along the sample ($E_0 = 3$ mJ). The arrow indicates the beam propagation direction.

Figure 1 shows an example of processing experimental data. Here, cases where the glass bar is exposed to a train of laser pulses with energies of 3 and 4.5 mJ are presented. These energies corresponded to average pulse powers of 70 and 100 GW, respectively, i.e., values exceeding the critical self-focusing power in glass by three orders of magnitude. Under these conditions, a laser pulse propagates in the MF regime with the formation of plasma channels practically throughout the entire sample length. The recombination de-excitation of these channels occurs in all directions, including the normal to the sample lateral face. As can be seen in Figs 1a and 1b, it is characterised by nonuniform brightness distribution both along and across the beam propagation direction.

We interpret the maxima in the longitudinal and transverse profiles of relative brightness J of the image as the luminescence from individual plasma channels, which accompany individual light filaments in the laser beam. An analysis of the data in Fig. 1c and the corresponding inset suggests that the transverse size of the plasma channels formed at different points of the glass bar is characterised by high stability, whereas the channel length varies in rather wide limits.

Since glass is transparent in its luminescence spectral range, the CCD matrix camera records the total radiation emitted throughout the entire volume of the glass bar. Therefore, the plasma-channel length, determined from the longitudinal profile of the plasma-region luminescence brightness, is a conditional value to some extent because of possible superposition of the images of channels located at different depths in the glass. The real channel length could not be estimated in our experiments without physical destruction of the sample (note that the use of a wedge-shaped sample partially removes this problem [20]). For this reason, this problem was solved by numerical simulation of the MF of an ultrashort laser pulse in quartz glass (see results below).

At the same time, the lateral-luminescence images of the glass bar can be used to characterise fairly exactly the change in the linear density of the total number of plasma channels, n_f, formed within the filamentation zone. To this end, one must perform numerical integration of channel brightness J along vertical grid lines:

$$S_J(z_i) = \Delta y \sum_{j=1}^{N_y} J_{ij},$$

where J_{ij} is the brightness at a point with coordinates z_i and y_j; and N_y and Δy are, respectively, the grid dimension and size along the y axis. The dependence of the total brightness (normalised to its maximum) on z is shown in Fig. 1d.

It can be seen in Fig. 1d that the total brightness of the plasma-channel image has a pronounced main maximum, which is somewhat shifted with respect to the filamentation zone centre (the point in the spatial region from which the glass bar luminescence is recorded) toward the bar input face. This maximum is a manifestation of the crowding of the number of channels near the beam optical axis; as will be shown below, it corresponds to the nonlinear focus of the laser beam (global nonlinear focus). The tail of the dependence $S_j(z)$ is rather flat and contains separated local maxima, which are formed (as follows from Fig. 1a) by peripheral (relative to the optical axis) plasma channels.

An increase in the input radiation energy (Fig. 1b) leads to elongation of the plasma luminescence region (i.e., the filamentation zone) in the glass bar and increases the number of newly formed plasma channels. The corresponding dependences are shown in Fig. 2.

The length of the entire beam-filamentation zone L_{pl} was estimated from the plasma-luminescence brightness histograms (similar to the longitudinal profile $J(z)$ presented in Fig. 1c) at a level of 1% of the maximum.

The number of plasma channels n_f was determined as the total number of local luminescence brightness maxima in the recorded images of the plasma region in the sample. The results were averaged over a series of several tens of single pulse shots.

It is of interest that, at pulse powers $P_0 > 70$ GW, plasma channels were observed practically throughout the entire length of the glass bar. As can be seen in Fig. 2a, the increase in the effective filamentation length with an increase in power was small. At the same time, the total number of newly formed plasma channels increases significantly under at the same observation conditions (Fig. 2b). This fact suggests expansion of the plasma-formation region away from the optical axis of the laser beam with an increase in its power and involvement of its peripheral regions into filamentation.

Figures 1a and 1b demonstrate also the effect of successive refocusings of the optical field of the pulse during its filamentation in the quartz glass. Indeed, let us consider Fig. 3, which shows (on the enlarged scale) a small portion of the glass bar with luminous plasma channels. Here, one can select some groups of channels (e.g., three enumerated channels)

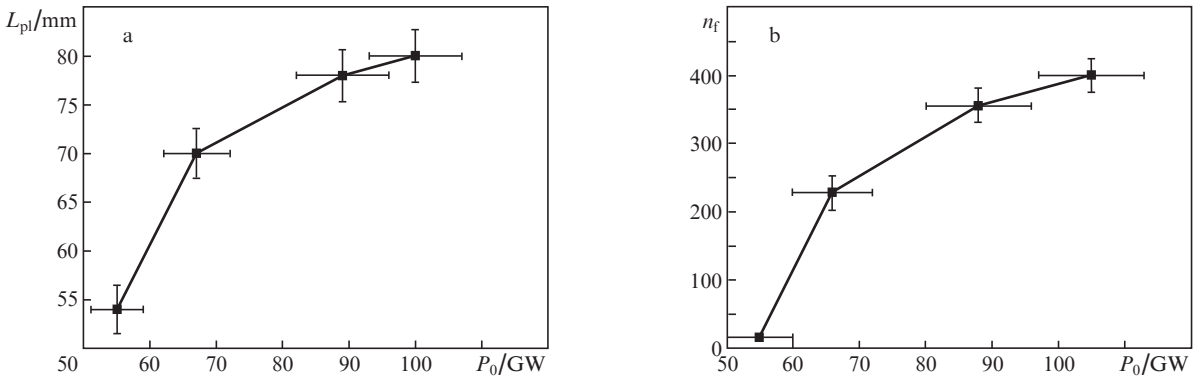

Figure 2. Dependences of the (a) effective length L_{pl} of plasma-formation region and (b) total number of plasma channels n_f on laser pulse power P_0.

that are located on one straight line along the beam propagation direction. These channels have generally different lengths and thicknesses; however, by analogy with the results of single-filamentation studies [17, 18], one can suggest that they all are formed as a result of successive refocusing cycles of the optical field of the same filament. These filament oscillations are due to the instability of the dynamic balance between the focusing optical nonlinearity of the medium (Kerr self-focusing) and the physical mechanisms leading to beam defocusing, such as the nonlinear absorption at photoionisation and refraction in the self-induced plasma. The number of these successive filament refocusings increases with an increase in the laser pulse energy, while the length of individual plasma channels decreases under these conditions [17]. For convenience, we will refer to the plasma channels formed successively by the same filament as channel generations; they will be enumerated successively, as in Fig. 3.

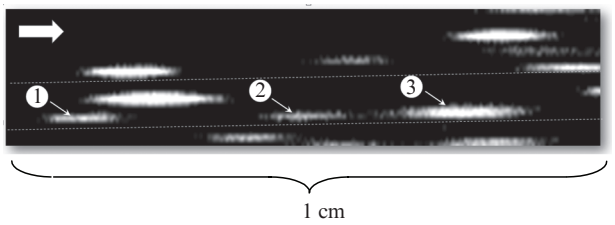

Figure 3. Enlarged image of plasma channels in a glass bar. Successive pulse refocusings are enumerated. The arrow indicates the beam propagation direction.

3. Numerical model of laser pulse filamentation

The above experimental data make it possible to reveal general properties of self-focusing and filamentation of ultrashort laser pulses (USLPs) in a nonlinear medium and obtain quantitative information about the position and density of plasma channels inside a transparent dielectric. However, the evolution of laser beam MF and the fine structure of the plasma-formation region cannot yet be studied experimentally; thus, one has to simulate numerically the physical process under study.

The theoretical simulation of the nonlinear propagation of gigawatt USLPs in a dielectric is generally based on the equation of paraxial optics and takes into account the nonlinear response of the material. We will consider this equation as a nonlinear Schrödinger equation (NSE) in the four-dimensional space–time continuum. To make a full description of laser pulse MF, one must calculate the spatial and temporal dynamics of the pulse optical field along all coordinates, with allowance for the optical nonlinearity of the medium (Kerr effect), its photoionisation and the formation of plasma regions. The NSE approach allows one to correctly take into account, along with linear effects (diffraction, absorption), the 'temporal memory' of the propagation medium, which is related to the frequency dispersion of the temporal profile of light pulse, inertia of cubic nonlinearity (Raman scattering), and the nonstationary character of plasma defocusing [2, 21].

The NSE used to simulate numerically the MF in quartz can be written in the form [22]

$$\left(\frac{\partial}{\partial z}-\frac{\mathrm{i}}{2n_0k_0}\nabla_\perp^2+\frac{k_\omega''}{2}\frac{\partial^2}{\partial t^2}\right)U=\mathrm{i}k_0(\tilde{n}_2+n_{\mathrm{pl}})\,U-\alpha_{\mathrm{NL}}\,U\,. \quad (1)$$

Here, U is the field amplitude; $\nabla_\perp^2=\partial^2/\partial x^2+\partial^2/\partial y^2$ is the transverse Laplacian; n_0 is the linear refractive index of the medium; $k_0=2\pi/\lambda_0$ is the wave number; $I=cn_0|U|^2/(8\pi)$ is the pulse intensity; c is the speed of light in vacuum; $k_\omega''=\partial^2k/\partial\omega^2$ is the second-order dispersion coefficient of the light pulse group velocity in the medium; $\tilde{n}_2(t)$ is the effective coefficient of cubic (Kerr) nonlinearity with allowance for the response inertia [22]; $n_{\mathrm{pl}}=-\rho_{\mathrm{e}}/(2\rho_{\mathrm{c}}n_0)$ is the 'plasma' nonlinearity coefficient; $\rho_{\mathrm{c}}=1/(\sigma_{\mathrm{c}}\tau_{\mathrm{c}}c)$ is the critical plasma electron density; $\alpha_{\mathrm{NL}}=\sigma_{\mathrm{c}}\rho_{\mathrm{e}}/2+(2I)^{-1}W_IE_{\mathrm{i}}(\rho_{\mathrm{nt}}-\rho_{\mathrm{e}})$ is the nonlinear absorption coefficient of the medium; σ_{c}, τ_{c}, and E_{i} are, respectively, the cascade ionisation cross section, the electron mean free time and the dielectric band gap; and W_I is the photoionisation probability of a material with a concentration of neutral atoms (molecules) ρ_{nt}.

The evolution of the concentration ρ_{e} of light-induced free electrons in a laser-beam channel obeys the following simplified kinetic equation [23], with allowance for the implementation of field (multiphoton) and collisional (avalanche) ionisation regimes in the material:

$$\frac{\partial\rho_{\mathrm{e}}}{\partial t}=W_I(I)(\rho_{\mathrm{nt}}-\rho_{\mathrm{e}})+(\nu_{\mathrm{i}}-\nu_{\mathrm{r}})\rho_{\mathrm{e}}, \quad (2)$$

where ν_{i} and ν_{r} are, respectively, the effective impact ionisation and recombination rates. In the Drude approximation [2], where the free-electron-velocity distribution is disregarded, and some electrons averaged over kinetic energies and having a mean constant transit time τ_{c} between collisions are considered, the electron-impact ionisation rate of the atom (ν_{i}) depends linearly on the light-wave intensity and cascade ionisation cross section σ_{c}: $\nu_{\mathrm{i}}=I(\boldsymbol{r},t)\sigma_{\mathrm{c}}/E_{\mathrm{i}}$. The free-electron recombination rate ν_{r} in a solid dielectric is generally assumed to be constant.

The model medium was chosen to be fused silica. The optical properties of this material are similar to those of the BK7 glass used in our experiments (see, for example, [24]); however, fused silica is much more completely certified in the scientific literature. The main parameters of the above-described numerical model for fused silica in the region of the main harmonic of Ti : sapphire laser ($\lambda_0=800$ nm) were taken from [23, 25].

To provide small-scale MF in numerical calculations, we set the initial laser beam profile using a model ideal Gaussian beam $[u_{\mathrm{G}}(\boldsymbol{r}_\perp)]$ in the spatial–temporal continuum, with imposed random amplitude and phase noise of the light field:

$$u(\boldsymbol{r}_\perp,z=0)=u_{\mathrm{G}}(\boldsymbol{r}_\perp)+A\tilde{u}_{\mathrm{rnd}}(\boldsymbol{r}_\perp).$$

Here, $u=U/U_0$ is the complex amplitude of the light-pulse electric field, normalised to the initial value U_0 (it is a function of transverse coordinates $\boldsymbol{r}_\perp\equiv\{x,y\}$ and evolution variable z);

$$u_{\mathrm{G}}(\boldsymbol{r}_\perp)=\exp\{-[|\boldsymbol{r}_\perp|/(2a_0)]^2\}\exp[-\mathrm{i}(2k_0|\boldsymbol{r}_\perp|^2/f)];$$

a_0 is the beam radius at a level of 1/e; f is the initial radius of curvature of the beam phase front (in the case under consideration, one always has $f\to\infty$); and $\tilde{u}_{\mathrm{rnd}}$ is a two-dimensional random (complex) noise with a normal distribution, zero mean and a unit peak amplitude. The scale coefficient A was 0.1. All numerically obtained parameters were statistically

averaged over ten independent calculations of the model problem (with other conditions invariable).

The photoionisation rate was calculated using the well-known Keldysh multiphoton ionisation model [26]. The quartz band gap was chosen to be 9 eV [23]; this value call for six optical field photons to be absorbed to transfer a bound electron to the valence band.

4. Structural characteristics of MF

Let us consider the characteristics of the plasma region formed in the bulk of fused silica irradiated by a femtosecond laser pulse. It was impossible to calculate numerically the filamentation dynamics for the real (used in our experiments) laser beam (with an initial radius $R_0 \approx 3$ mm) because of the well-known problem of extremely stringent requirements to the dimension of the four-dimensional numerical matrices storing the complex optical-field amplitudes at each point of the optical path. For this reason, we have numerically simulated MF for a laser beam scaled to smaller diameters. As a result, we could not perform direct numerical interpretation of the experimental data; nevertheless, the simulation allowed us to reproduce the main qualitative regularities of the filamentation evolution in the bulk of nonlinear medium. All calculations were performed for a beam with an initial radius $R_0 = 0.1$ mm and a pulse width of 45 fs. Correspondingly, we diminished the maximum laser pulse energy (to 80 μJ) and the reduced-power parameter $\eta = P_0/P_e$.

The 3D images of plasma channels, presented in Fig. 4 in the form of surfaces of equal free-electron concentration ($\rho_e = 10^{13}$ cm^{-3}) for two pulse energies E_0, describe qualitatively the MF process. Figures 4a and 4b show also the spatial distributions (in the form of continuous-tone volume figures) of the light energy density $w(x, y, z)$ for a pulsed laser beam passing through a quartz bar. It can be seen that an increase in the pulse energy, which is equivalent to an increase in peak power P_0 within the numerical experiment, leads to evolution of the newly formed plasma region along all spatial coordinates: the total length of the domain of existence of plasma channels increases, and its area in the transverse direction increases as well. For a relatively low pulse energy, $E_0 = 10$ μJ ($\eta = 62$), there are only few (about five) plasma channels in the quartz sample; the longest is located near the laser beam axis and is characterised by longitudinal connectivity on a length of about 0.5 cm.

An increase in the beam energy to 30 μJ ($\eta = 187$) (i) approaches the plasma formation point to the input face of the sample and (ii) leads to rapid generation of free charges throughout the entire beam cross section rather than on only the beam axis. This pattern, being in complete agreement with the qualitative conclusions based on experimental data, is confirmed by the dependences shown in Fig. 2. The total number of the plasma channels formed throughout the entire extent of the filamentation zone is approximately an order of magnitude larger than for a low-energy pulse, and the plasma channels are on average shorter; this is caused by the decrease in the spatial sizes of the laser beam profile inhomogeneities, which is sufficient for developing local (small-scale) beam self-focusing. Another characteristic distinctive feature of these images is that the longitudinal distribution of the number of plasma channels is significantly nonuniform for $E_0 = 30$ μJ. In fact, one can state that an increase in E_0 causes grouping of plasma regions in the initial portion of the light beam path.

Let us now analyse quantitatively the above-considered regularities. To calculate the MF statistics, we made it possible to trace the entire life cycle of individual plasma channels formed in a quartz sample in our numerical experiments. This procedure was implemented as follows.

The two-dimensional distribution of the concentration of free plasma electrons, $\rho_e(x, y, z)$, steady by the end of laser pulse, was calculated at each point of the optical path at all points of the transverse grid. Then this distribution was binarised with respect to some specified threshold level ρ_{e1}. The resulting array of binary values was analysed (using a two-pass ABC algorithm [27]) for the presence of connected regions (CRs), which were considered as projections of individual plasma channels onto a specified cross section. A unique index was assigned to each such region, and the spatial characteristics of the latter (position, area, and rms sizes over axes) were compared with the corresponding parameters of plasma channels, saved in a special database in the previous spatial step.

Longitudinal step-by-step tracing of connected regions (channels) was based on the assumption of small displacement of the centroid of region chosen from its position at the

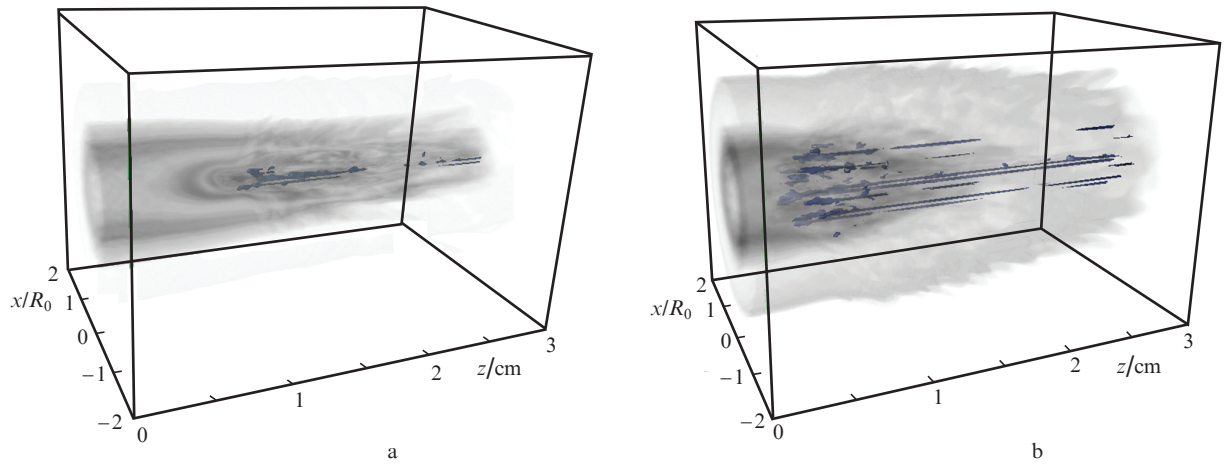

Figure 4. Isosurfaces of $\rho_e = 10^{13}$ cm^{-3} and laser beam energy density (continuous-tone figures) upon filamentation in a $(0.4 \times 0.4 \times 30)$-mm quartz bar for E_0 = (a) 10 and (b) 30 μJ. The beam propagates from left to right.

previous step. This means that the longitudinal coordinate is used to calculate the coordinates of the centroid and rms radius of each CR found at each next computation step. Then displacement d of the centroid of each such region from the position r_c of the centroid of each CR fixed at the previous step was calculated. Provided that $d \leqslant r_c$, it was assumed that the CR under consideration belongs to the plasma channel subjected to tracing. If this condition was not satisfied for some CR (or some CRs), this region was taken as a starting point for a new filament (plasma channel). The length of elementary plasma channels (L_{fm}) was calculated from the previously saved coordinates of their origins.

To enumerate the plasma channels (filaments) successively formed in a given CR, we introduced into consideration an integer index m, characterising the number of local field refocusings in a chosen area of beam cross section. In other words, if $m > 0$, a plasma channel with a specified electron concentration $\rho_e \geqslant \rho_{e1}$ arose and disappeared m times in a given CR during light beam evolution. For example, the pattern in Fig. 5 exhibits the formation of five successive plasma channels in some chosen CR, which are denoted as PCh_m (m is the serial number of plasma channel). At the final point of the beam path, the matrices containing lengths and starting coordinates of filaments were statistically processed to calculate the mean values and range of variation in parameters.

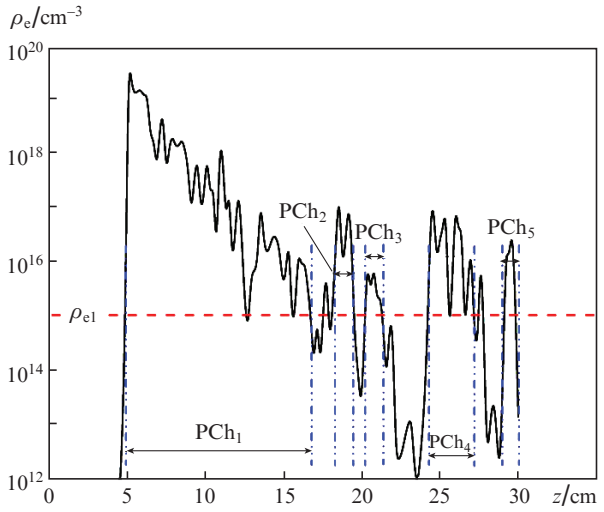

Figure 5. Example of evolution of peak free-electron concentration ρ_e at some fixed point of the transverse beam profile along the beam propagation path. The characteristic filamentation level ρ_{e1} and the arrangement of generations of plasma channels (PCh_m) are shown.

The above-described procedure of determining the number of isolated filamentation zones is illustrated in Fig. 6, which shows the transverse arrangement of the plasma channels arising in quartz at different distances. The images were constructed by transforming the real profile of the free-electron concentration $\rho_e(x,y)$ into a binary distribution $A(x,y)$ based on the condition $\rho_e > \rho_{e1}$, where $\rho_{e1} = 10^{15}$ cm^{-3}. This value was chosen proceeding from the experimental data on the fluorescence of plasma channels in gases with an average free-electron concentration on the order of $10^{13}-10^{15}$ cm^{-3} [2]. Both individual plasma channels and groups of closely spaced channels are shown as dark spots in Fig. 6. Depending on the longitudinal coordinate, the total number of channels in the quartz bar may change; however the characteristic groups of channels (examples are those successively enumerated in Fig. 6) retain their position in the beam throughout the entire propagation path. In this numerical realisation, an individual plasma channel, evolving along the propagation path, could change its transverse half-width in the range of 4–10 μm, which corresponds to a similar range of transverse coordinates of computational grid points.

Obviously, the approach used by us does not quite correctly takes into account the situation with closely spaced plasma channels; in this case, neighbouring projections of channels (spots) coalesce in binarised profiles of the free electron concentration. For example, a rather large spot with number 1 in Fig. 6a is divided into two smaller spots (individual plasma channels) with numbers 1 and 2 (Figs 6b, 6c) when moving along the propagation path. The numerical algorithm would interpret this fact as the occurrence of a new channel near the initial one with an increase in the channel number counter by unity, although one can suggest that there were two closely spaced channels initially. Nevertheless, we expect this ambiguity to lead to only a small error in our estimates, because the total number of newly formed plasma channels is fairly large.

Let us now turn to Fig. 7, which shows functional dependences of the parameters characterising the laser pulse MF in a medium: number of plasma channels n_f and their length L_f.

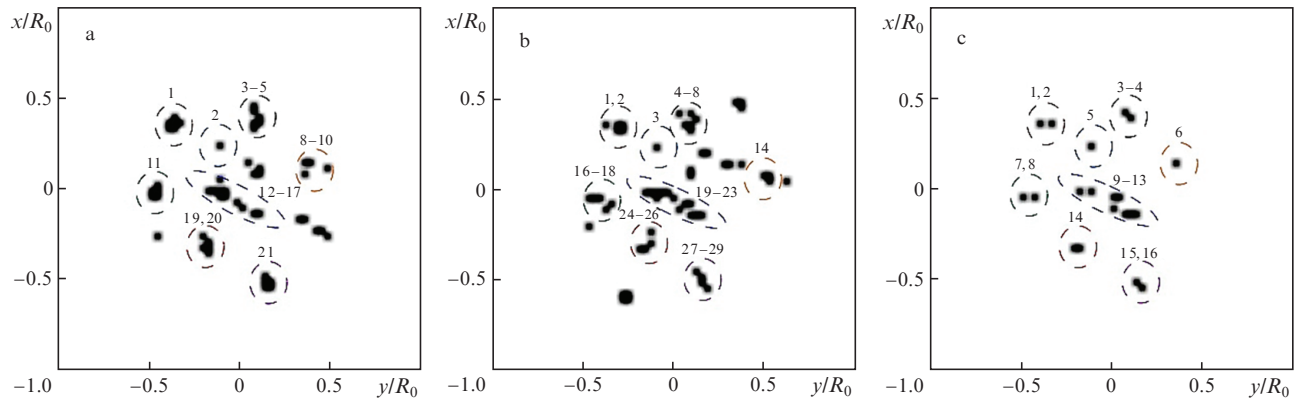

Figure 6. Spatial distribution of plasma channels $A(x,y)$ over the laser beam cross section ($E_0 = 30$ μJ) at distances of $z =$ (a) 5, (b) 7 and (c) 20 mm. Characteristic groups of channels are selected and enumerated.

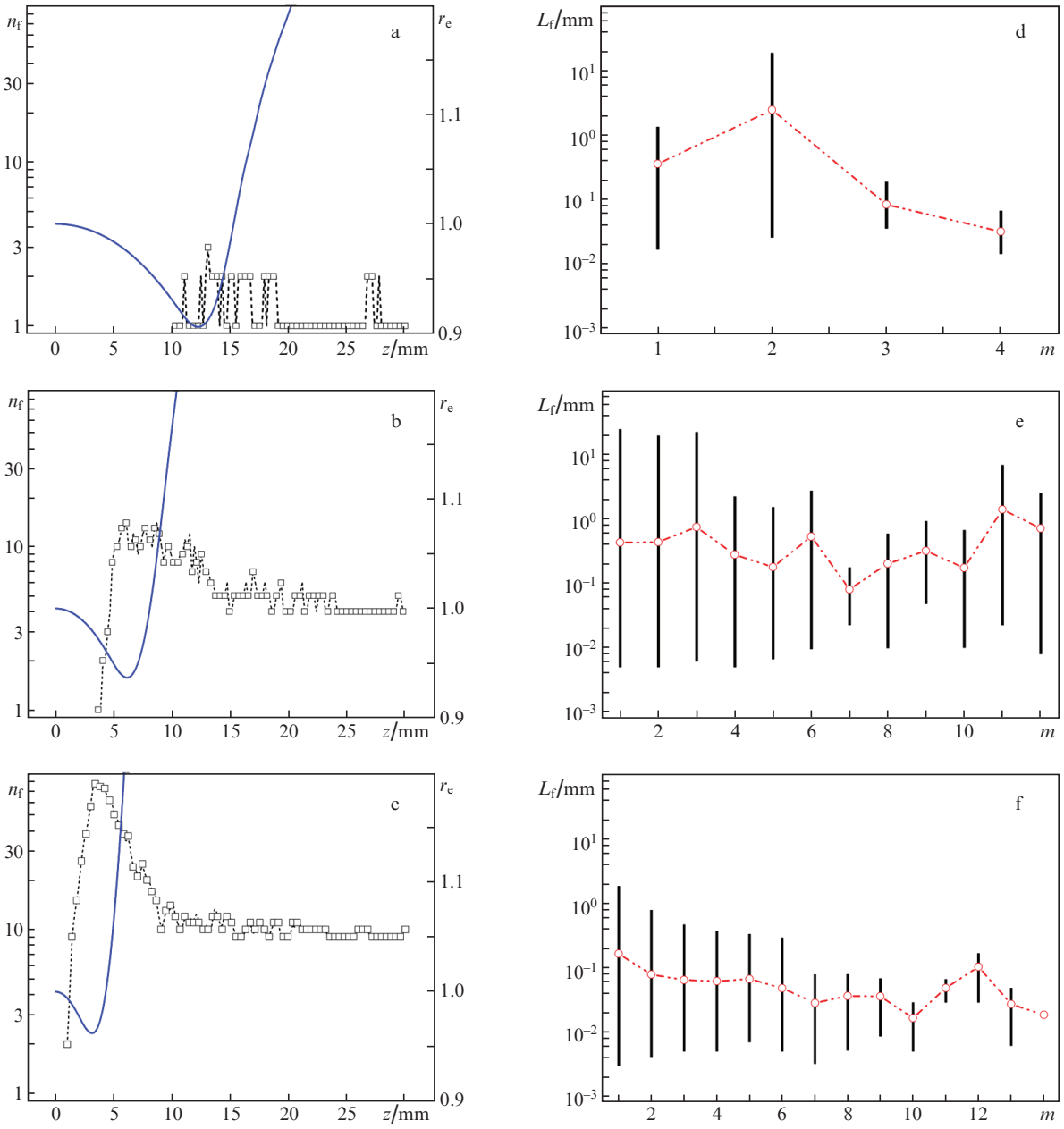

Figure 7. (a–c) Number of plasma channels n_f (symbols) and normalised effective beam radius $r_e = R_e/R_0$ (solid lines) along the optical path and (d–f) channel length L_f as a function of channel generation index m at E_0 = (a, d) 10, (b, e) 30 and (c, f) 80 μJ.

A comparison of the dependences of n_f in Figs 7a–7c shows that a rise in E_0 causes structural changes in the plasma region (in the part where beam filamentation occurs): its effective length increases, and the number of newly formed channels sharply rises. At the same time, the aforementioned effect of plasma-channel grouping is pronounced in the dependences $n_f(z)$. The number of plasma channels was found to be maximal near the coordinate of global nonlinear focus of the beam, z_g, which is defined as the coordinate of the minimum in the longitudinal dependence of rms (effective) beam radius R_e [28]:

$$R_e(z) = \left[E^{-1}(z)\int_T \mathrm{d}t \iint_{\boldsymbol{R}_\perp} \mathrm{d}^2\boldsymbol{r}_\perp I(\boldsymbol{r}_\perp, z; t)\left|\boldsymbol{r}_\perp - \boldsymbol{r}_{gr}(z)\right|^2\right]^{1/2}, \quad (3)$$

where $E(z)$ is the pulse energy at the point z and $\boldsymbol{r}_{gr}$ is the radius vector of the beam centroid [with respect to beam intensity $I(\boldsymbol{r}_\perp, z; t)$]. The integration in (3) is over the entire calculation domain, including the time (T) and transverse spatial ($\boldsymbol{R}_\perp$) grids. The dependences of the relative value $r_e(z) = R_e(z)/R_0$ are also shown in Fig. 7.

In the theory of aberration-free stationary self-focusing of a light beam [29], the evolution of the beam effective radius to the point of its transverse collapse is set by a simple relation:

$$R_e(z) = R_e(z=0)\sqrt{1 + (1-\eta)(z/L_d)^2}, \quad (4)$$

where parameter $L_d = k_0 R_0^2$ is the diffraction length of the beam. It was shown in [30] that this law is also valid for the more realistic case of laser pulse single filamentation, pro-

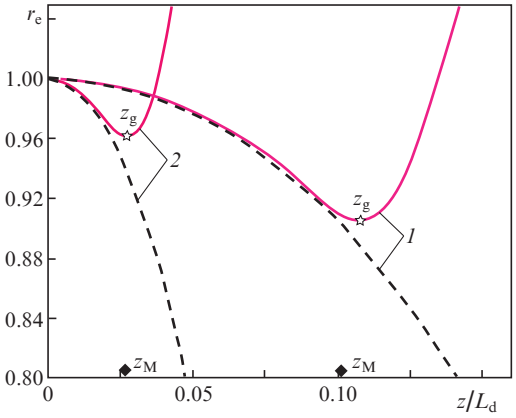

Figure 8. Longitudinal evolution of the effective radius $r_e(z)$, normalised to its initial value, for pulse energies $E_0 = (1)$ 10 and (2) 30 μJ, calculated using the numerical model (1), (2) (solid lines) and based on formula (4) (dashed lines).

vided that one corrects the reduced radiation power: $\eta \to \eta^* = \eta/b$, where $b > 1$ is some empirical fitting parameter, which takes into account the temporal pulse profile.

Surprisingly, formula (4) also holds true for the MF regime considered here. Indeed, as follows from Fig. 8, the dependence of the aberration-free rms beam radius (3) on the longitudinal coordinate describes fairly exactly the real dependence $R_e(z)$ obtained from numerical calculations if one takes $b \approx \sqrt{2}$. A correlation is observed for different pulse energies (powers) and, as it was suggested, exists only up to the vicinity of the global focus coordinate z_g, denoted by an asterisk in Fig. 8.

It is important to know the coordinate of the global beam focus, because specifically in this region (see above) the number of filaments and corresponding plasma channels is maximal. One cannot determine a priori the coordinate z_g of laser-beam global focus without solving numerically the complete problem (1), (2). However, as our investigations showed, the z_g value can be estimated with an error of about 10% using the well-known Marburger formula [31],

$$z_g \approx z_M(\eta^*) = \frac{0.367 L_d}{\sqrt{\left(\sqrt{\eta^*} - 0.852\right)^2 - 0.0219}}, \qquad (5)$$

at $\eta^* > 1$ and with the real peak power of laser pulse corrected using parameter b. Despite the fact that this expression was initially obtained as an approximation of data calculated along the self-focusing length in the regime of a single axial filament, it can be applied to MF. This is evidenced by Fig. 8, where starting filamentation coordinates z_M for a collimated laser beam, which were calculated from formula (5), are shown.

Let us now turn to Figs 7d–7f, which show the evolution of the length of elementary plasma channels with an increase in the generation serial number m. The vertical lines indicate the range of variation in the parameter L_f for each generation of channels. The points connected by lines correspond to ensemble-averaged realisations of values. For example, one can see that, in the case of moderate laser pulse energy (Fig. 7d), the first few generations of plasma channels are characterised by a larger spread of lengths (approximately from 6 μm to almost 24 mm) than the next generations. These channels are formed at different points along the beam propagation path in the quartz sample and at different points of the beam cross section. The next generations contain plasma channels characterised by a diminishing (generally) spread of L_f values; however, the channel length changes on average irregularly from generation to generation. This tendency can clearly be seen in all the dependences discussed above; it was also indicated previously in [17].

The number of filament generations and the number of shorter plasma channels in each generation increase with increasing pulse energy. An analysis of our data on the change in the length of the plasma channels formed at different points of the laser beam cross section (omitted here) showed that short-lived channels are generally formed at the beam periphery, where initial local perturbations of the transverse profile of optical field amplitude (seeds of future filaments) contain low partial power. The closer they are positioned to the beam centre, the higher the power in these perturbations is (because of the Gaussian envelope of the intensity profile) and the more actively and earlier the self-focusing and filamentation of these beam regions occur. In total, this circumstance would lead to a larger number of spatially local refocusings [17] in the central regions of the beam in comparison with its periphery and, on the whole, to longer plasma channels. In other words, the physical nature of the phenomena under consideration is the initially nonuniform energy (power) distribution over the laser beam cross section, which gives rise to differences in the coordinates of filamentation onset in the centre and at the periphery of the beam and in the number of local field refocusings (and, correspondingly, in the total length of plasma channels).

5. Conclusions

We performed an experimental and theoretical study of the spatial structure of the plasma region formed by a high-power USLP (λ_0 = 800 nm) during its nonlinear propagation in a transparent dielectric in the MF regime. The statistics of the filament formation and the parameters of MF-zone microstructure were analysed by tracing the entire life cycle of individual plasma channels formed in the sample bulk, taking into account repeated beam refocusings (generations of channels). The dependences of the number, position, and length of plasma channels on the pulse energy were obtained.

The investigations revealed that, despite the dynamic and absolutely random character of MF, this regime of USLP self-action exhibits also some regular features of its evolution. In particular, we found close-to-unimodal distribution of the number of plasma channels over the dielectric sample length; the position of the distribution peak correlates on the whole with the position of the laser beam nonlinear focus. In addition, an increase in the laser beam energy is accompanied by pronounced evolution of the arising plasma region along all spatial coordinates (the region elongates, and its cross section increases) and an increase in the number of newly formed generations of channels. The extent of these channels is characterised by a large spread of values in each generation; however, one can state that, the higher the laser pulse power, the shorter (on average) the forming plasma channels.

Acknowledgements. We are grateful to D.V. Apeksimov (V.E. Zuev Institute of Atmosphere Optics, Siberian Branch, Russian Academy of Sciences) and A.Yu. Maior (Institute of Automatics and Control Processes, Far Eastern Branch, Russian Academy of Sciences) for their help in the prepara-

tion and performance of experiments and fruitful discussions of the results. We also highly appreciate the helpful remarks and advice of V.P. Kandidov (Moscow State University), which made it possible to improve radically our paper.

This work was supported by the Russian Foundation for Basic Research (Grant No. 14-28-02023 ofi_m) and the Russian Science Foundation (Agreement No. 15-17-10001).

References

1. Askar'yan G.A. *Zh. Eksp. Teor. Fiz*., **42**, 1567 (1962).
2. Shen Y.R., Boyd R.W., Lukishova S.G. (Eds) *Self-focusing: Past and Present* (New York: Springer, 2009).
3. Chekalin S.V., Kandidov V.P. *Usp. Fiz. Nauk*, **183**, 133 (2013).
4. Houard A., Liu Y., Mysyrowicz A. *J. Phys. Conf. Ser*., **497**, 012001 (2014).
5. Bespalov V.I., Talanov V.I. *Pis'ma Zh. Eksp. Teor. Fiz*., **3** (2), 471 (1966).
6. Mlejnek M., Kolesik M., Moloney J.V., Wright E.M. *Phys. Rev. Lett*., **83**, 2938 (1999).
7. Liu W., Hosseini S.A., Luo Q., Ferland B., Chin S.L., Kosareva O.G., Panov N.A., Kandidov V.P. *New J. Phys*., **6**, 6 (2004).
8. Chin S.L., Petit S., Liu W., Iwasaki A., Nadeau M.-C., Kandidov V.P., Kosareva O.G., Andrianov K.Yu. *Opt. Commun*., **210**, 329 (2002).
9. Chin S.L., Talebpour A., Yang J., Petit S., Kandidov V.P., Kosareva O.G., Tamarov M.P. *Appl. Phys. B*, **74**, 67 (2002).
10. Paunescu G., Spindler G., Riede W., Schröder H., Giesen A. *Appl. Phys. B*, **96**, 175 (2009).
11. Berge L., Skupin S., Lederer F., Mejean G., Yu J., Kasparian J., Salmon E., Wolf J.P., Rodriguez M., Woste L., Bourayou R., Sauerbrey R. *Phys. Rev. Lett*., **92**, 225002 (2004).
12. Hosseini S.A., Luo Q., Ferland B., Liu W., Chin S.L., Kosareva O.G., Panov N.A., Aközbek N., Kandidov V.P. *Phys. Rev. A*, **70**, 033802 (2004).
13. Shlenov S.A., Kandidov V.P. *Opt. Atmos. Okeana*, **17**, 637 (2004).
14. Zvorykin V.D., Ionin A.A., Levchenko A.O., Seleznev L.V., Sinitsyn D.V., Smetanin I.V., Ustinovskii N.N., Shutov A.V. *Plasma Phys. Rep*., **41**, 112 (2015).
15. Schroeder H., Chin S.L. *Opt. Commun*., **234**, 399 (2004).
16. Hao Z., Stelmaszczyk K., Rohwetter P., Nakaema W.M., Woeste L. *Opt. Express*, **19**, 7799 (2011).
17. Yang J., Mu G. *Opt. Express*, **15**, 4943 (2007).
18. Dharmadhikari A.K., Dharmadhikari J.A., Mathur D. *Appl. Phys. B*, **94**, 259 (2009).
19. Geints Yu.E., Apeksimov D.V., Afonasenko A.V. *Programmno-vychislitel'nyi kompleks dlya analiza poperechnykh profilei lazernykh puchkov (profilometr)* (Software Package for Analysing Transverse Laser Beam Profiles (Profiler)). Certificate of Governmental Registration No. 2014616871 (2014).
20. Kandidov V.P., Smetanina E.O., Dormidonov A.E., Kompanets V.O., Chekalin S.V. *Zh. Eksp. Teor. Fiz.*, **140**, 484 (2011).
21. Geints Yu.E., Zemlyanov A.A., Kabanov A.M., Matvienko G.G. In: *Nelineinaya femtosekundnaya optika atmosfery* (Nonlinear Femtosecond Optics of Atmosphere) (Tomsk: Izd-vo Inst. Optiki Atmosfery SO RAN, 2010).
22. Geints Yu.E., Bulygin A.D., Zemlyanov A.A. *Appl. Phys. B*, **107**, 243 (2012).
23. Couairon A., Sudrie L., Franco M., Prade B., Mysyrowicz A. *Phys. Rev. B*, **71**, 125435 (2005).
24. Lu X., Liu Q., Liu Z., Sun S., Ding P., Ding B., Hu B. *Appl. Opt*., **51**, 2045 (2012).
25. Kosareva O.G., Nguyen T., Panov N.A., Liu W., Saliminia A., Kandidov V.P., Akozbek N., Scalora M., Vallee R., Chin S.L. *Opt. Commun*., **276**, 511 (2006).
26. Keldysh L.V. *Zh. Eksp. Teor. Fiz*., **47**, 1945 (1964).
27. http://habrahabr.ru/post/119244/.
28. Zemlyanov A.A., Geints Yu.E. *Opt. Spektrosk*., **104**, 852 (2008).
29. Vlasov S.N., Petrishchev V.A., Talanov V.I. *Radiophys. Quantum Electron*., **14**, 1062 (1971).
30. Zemlyanov A.A., Geints Y.E. *Eur. Phys. J. D*, **42**, 349 (2006).
31. Marburger J.H. *Prog. Quantum Electron*., **4**, 35 (1975).